Subphase transitions in first-order aggregation processes

Tomas Koci and Michael Bachmann

Phys. Rev. E **95**, 032502 — Published 8 March 2017

DOI: 10.1103/PhysRevE.95.032502

Subphase transitions in first-order aggregation processes

Tomas Koci[1,*] and Michael Bachmann[1,2,3,†]

[1] *Soft Matter Systems Research Group, Center for Simulational Physics, The University of Georgia, Athens, GA 30602, USA*
[2] *Instituto de Física, Universidade Federal de Mato Grosso, Cuiabá (MT), Brazil*
[3] *Departamento de Física, Universidade Federal de Minas Gerais, Belo Horizonte (MG), Brazil*

(Dated: February 7, 2017)

In this study, we investigate the properties of aggregation transitions in the context of generic coarse-grained homopolymer systems. By means of parallel replica-exchange Monte Carlo methods, we perform extensive simulations of systems consisting of up to 20 individual oligomer chains with 5 monomers each. Using the tools of the versatile microcanonical inflection-point analysis, we show that the aggregation transition is a first-order process consisting of a sequence of subtransitions between intermediate structural phases. We unravel the properties of these intermediate phases by collecting and analyzing their individual contributions towards the density of states of the system. The central theme of this systematic study revolves around translational entropy and its role in the striking phenomena of *missing* intermediate phases. We conclude with a brief discussion of the scaling properties of the transition temperature and the latent heat.

PACS numbers: 05.70.Fh, 64.60.De, 64.70.-p, 82.35.Lr, 83.10.Tv

I. INTRODUCTION

Deeper understanding of aggregation processes in the context of microscopic molecular systems is relevant for a number of technological and biomedical applications. For example, protein aggregation is believed to play a critical role during the onset of many prominent pathological conditions, such as cystic fibrosis, Alzheimer's and Parkinson's diseases [1, 2]. The staggering complexity of even the simplest molecular systems precludes the possibility of obtaining the relevant thermodynamic quantities through direct analytical calculations [3]. Over the past two decades, the enormous increase in the availability of computational resources, together with significant progress in algorithmic developments, resulted in a vast number of computational studies on the thermodynamic and structural properties of complex microscopic systems. Among the most efficient simulation methods are the generalized-ensemble Monte Carlo algorithms, such as simulated tempering [4, 5], replica-exchange parallel tempering [6–9], multiple Gaussian modified ensemble (MGME) [10], together with multicanonical [11–16] and Wang-Landau sampling [17–19]. These have been applied successfully in numerous studies of structural phases and transition properties [20–31], surface adsorption [32–41], and aggregation [42–47] of generic off-lattice homopolymers and heteropolymers. The folding properties of coarse-grained protein models have also been examined extensively [48–54].

Importantly, despite the many advances in simulational methodologies, systematic studies of detailed atomistic models are well beyond current capabilities. However, it is a significant physical reality that many essential thermodynamic properties of complex systems are retained on larger than atomistic scales and can be well represented by coarse-grained models. In fact, coarse-graining is not just a concept to simplify modeling. It reflects inherent collective and cooperative behavior of constituents of systems on mesoscopic and macroscopic scales. This is intuitive since it is known that certain characteristic properties, such as the propensity towards aggregation, are often shared among diverse systems and hence cannot depend sensitively on microscopic details.

In mesoscopic systems, structure formation and phase-separation processes are fundamentally influenced by finite-size effects. Systematic statistical analysis approaches beyond the standard canonical methodology are needed to unravel the intricate details of the interplay between energy and entropy in finite systems. Due to the averaging process involved in the calculation of canonical quantities such as the ensemble energy or the heat capacity, specific features of structural transitions and phase properties are often lost [3]. This is remedied in more general approaches such as the Fisher partition zeros [55–58], or the microcanonical inflection-point analysis [59, 60].

This paper is organized as follows: In Sect. II, we introduce a coarse-grained model for interacting flexible elastic homopolymers, describe the employed computational methods, and briefly outline the methodologies of the microcanonical inflection-point analysis. In Sect. III, we present the simulational results for systems of up to $M = 20$ short polymer chains (oligomers). Based on the outcome of inflection-point analysis, we argue that the aggregation transition is a first-order process consisting of a sequence of subtransitions between intermediate structural phases. Next, we discuss why certain

* E-mail: koci@smsyslab.org
† E-mail: bachmann@smsyslab.org; Homepage: http://www.smsyslab.org

subphases are entropically more suppressed than others, and conclude with a brief excursion into the scaling properties of the aggregation transition temperature and the latent heat. Summary is provided in Sect. IV.

II. MODEL AND METHODS

In the following, we introduce a generic coarse-grained model for a system of interacting, flexible homopolymers. Coarse-grained models, with a suitably chosen set of parameters, drastically reduce computational complexity while preserving the essential structural and thermodynamic properties that are typically found in more complex models [61].

A. Standard model of interacting elastic chains

In this study, we investigate the aggregation of M interacting flexible oligomers, each composed of $N = 5$ monomers. During the simulations, the system is constrained inside of a steric sphere at a constant density of 10^{-3} monomers per unit volume. At this density the radius of the constraining sphere is larger than the length of the fully extended chains under investigation. The total energy of the system can be separated into intra-chain and inter-chain pairwise interactions

$$E_{\text{total}} = E_{\text{intra}} + E_{\text{inter}}. \tag{1}$$

The intra-chain contribution

$$E_{\text{intra}} = \sum_{k=1}^{M}\sum_{i=1}^{N-1} U_{\text{FENE}}(r_{ii+1}^{(k)}) + \sum_{k=1}^{M}\sum_{i<j}^{N} U_{\text{LJ}}^{\text{trunc}}(r_{ij}^{(k)}) \tag{2}$$

consists of both bonded and non-bonded interactions, where $r_{ij}^{(k)}$ is the distance between the pair of monomers (i,j) of the k-th chain. The first term contains the anharmonic finitely extensible nonlinear elastic (FENE) potential [62–64]

$$U_{\text{FENE}}(r_{ii+1}) = -\frac{K}{2}R^2 \ln\left[1 - \left(\frac{r_{ii+1} - r_0}{R}\right)^2\right], \tag{3}$$

with parameter values $K = 40$ and $R = 0.3$ as used in [65]. The second term represents the truncated and shifted Lennard-Jones (LJ) potential

$$U_{\text{LJ}}^{\text{trunc}}(r_{ij}) = \begin{cases} U_{\text{LJ}}(r_{ij}) - U_{\text{LJ}}(r_c), & \text{if } r_{ij} \le r_c, \\ 0, & \text{if } r_{ij} > r_c, \end{cases} \tag{4}$$

where

$$U_{\text{LJ}}(r_{ij}) = 4\epsilon\left[\left(\frac{\sigma}{r_{ij}}\right)^{12} - \left(\frac{\sigma}{r_{ij}}\right)^{6}\right]. \tag{5}$$

We set the energy scale ϵ to unity and the length scale to $\sigma = r_0/2^{1/6}$, where $r_0 = 0.7$ is the location of the LJ potential minimum. The cutoff radius is set to $r_c = 2.5\,\sigma$. The inter-chain contribution

$$E_{\text{inter}} = \sum_{k<l}^{M}\sum_{i,j}^{N} U_{\text{LJ}}^{\text{trunc}}(|\mathbf{r}_i^{(k)} - \mathbf{r}_j^{(l)}|), \tag{6}$$

consists solely of non-bonded LJ interactions. For the purpose of this study, all LJ interactions (intra- and inter-chain) have their parameters set to identical values.

B. Simulation methods

Relatively small polymer systems, consisting of $NM < 100$ monomers, can be conveniently simulated using parallel tempering, which is a generalized-ensemble replica-exchange Monte Carlo method [6–9] that can be easily implemented on parallel computer architectures. In larger systems, the density of states typically spans several thousand orders of magnitude, in which case the application of more sophisticated methods such as multicanonical sampling [11–16] or Wang-Landau [17–19] is more efficient. In this study we restrict our attention to systems consisting of up to 20 individual chains with 5 monomers each. The number of monomers per chain has been intentionally kept very low in order to enhance translational entropic effects which become more obscured by the impact of inherent conformational entropies as chain length is increased.

In a typical simulation, $R \approx 80$ replicas of the system were simulated in parallel at different temperatures in the range $T \in [0.1, 2.0]$. Single-monomer random displacement moves, restricted to a box of size l, were used to perform conformational updates for individual replicas. The proposed update was then accepted with the Metropolis probability

$$A_{\text{M}}\left(\mathbf{X}_{\text{old}} \to \mathbf{X}_{\text{new}}\right) = \min\left(1, e^{-\beta[E(\mathbf{X}_{\text{new}}) - E(\mathbf{X}_{\text{old}})]}\right), \tag{7}$$

where $\beta = 1/k_{\text{B}}T$ and $k_{\text{B}} \equiv 1$ in the simulation. The maximum magnitude of the displacement update l was adjusted individually for each temperature thread to achieve an average acceptance rate of $40 - 60\%$. Approximately every 100 Monte Carlo sweeps, an exchange of conformations between adjacent replicas i and j was proposed with the acceptance probability

$$A_{\text{PT}}\left(\mathbf{X}_i \leftrightarrow \mathbf{X}_j; \beta_i, \beta_j\right) = \min\left(1, e^{[\beta_j - \beta_i][E(\mathbf{X}_j) - E(\mathbf{X}_i)]}\right). \tag{8}$$

The temperature spacing between adjacent replicas was chosen to achieve an exchange probability exceeding 20%. This results in a higher density of replicas in the low-temperature region as well as near the locations of phase transitions. On average, 10^7 replica exchanges were performed, allowing for a total of 10^9 Monte Carlo sweeps per simulation.

C. Density of states and microcanonical analysis

As a result of parallel tempering simulations, each replica generates a canonical energy histogram $h(E,\beta_i)$, which is then used to calculate an estimate for the microcanonical density of states $g_i(E) \approx h(E,\beta_i)\exp(\beta_i E)$. Individual estimates $g_i(E)$ are only reliable for energies in the neighborhood of the peak of the canonical distribution obtained at the temperature β_i. Therefore a sufficient overlap between the histograms of neighboring replicas is necessary to ensure that an accurate estimate of the density of states can be obtained for the entire energetic range. To combine the histograms obtained from the individual temperature threads, we have used the weighted multiple-histogram method [66, 67], where the system of equations

$$\hat{g}(E) = \frac{\sum_{i=1}^{R} h(E,\beta_i)}{\sum_{i=1}^{R} M_i \hat{Z}_i^{-1} e^{-\beta_i E}}, \tag{9}$$

$$\hat{Z}_i = \sum_E \hat{g}(E) e^{-\beta_i E}, \tag{10}$$

must be solved iteratively until $\hat{g}(E)$ has converged.

The standard approach towards obtaining the thermodynamic properties of a polymer system is to perform a conventional analysis of energetic and structural fluctuating quantities in the canonical ensemble. Generally, peaks in the temperature derivative of a canonical expectation value

$$\frac{d}{dT}\langle O(\mathbf{X})\rangle(T) = \frac{1}{k_B T^2}[\langle O(\mathbf{X})E(\mathbf{X})\rangle(T) - \langle O(\mathbf{X})\rangle\langle E(\mathbf{X})\rangle(T)], \tag{11}$$

indicate extremal thermal activity in the system. However, the precise location of the transition points for finite systems depends on the choice of the thermodynamic observables and cannot be determined uniquely. If finite-size effects are significant, the identification of a structural transition can be difficult and underlying cooperative effects may entirely be smeared out in the averaging process.

It is therefore imperative to employ a more systematic approach towards the analysis of thermodynamic properties of finite systems, which is capable of uniquely identifying and classifying structural transitions of all orders. This is accomplished utilizing the inflection-point analysis in the microcanonical ensemble [3, 59]. The central quantity, containing virtually all information about the intricate interplay between entropy and energy, is the microcanonical inverse temperature defined as

$$\beta(E) = \frac{dS(E)}{dE}, \tag{12}$$

where

$$S(E) = k_B \ln g(E) \tag{13}$$

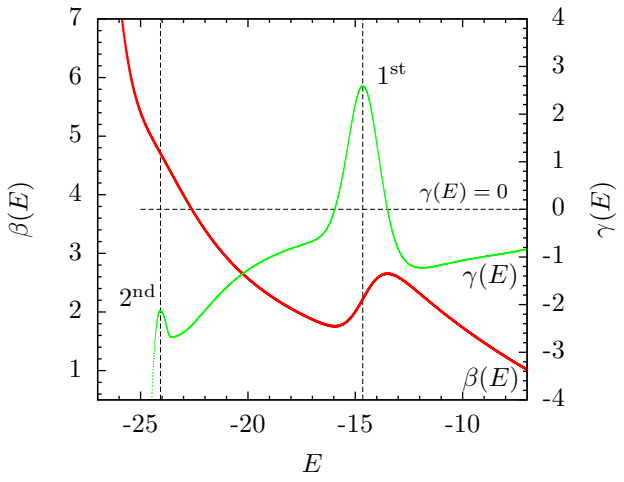

FIG. 1. Schematic illustration of microcanonical inflection-point analysis for the inverse microcanonical temperature $\beta(E)$. The prominent back-bending region in $\beta(E)$, together with the positive-valued peak in its energy derivative $\gamma(E)$ at $E \approx -15$, indicates a *first-order* transition. The negative-valued peak at $E \approx -24$ corresponds to a *second-order* transition.

is the microcanonical entropy and $g(E)$ is the density of states. In analogy to the principle of minimal sensitivity [68], structural transitions occur if $\beta(E)$, or one of its energy derivatives, responds least sensitively to variations in energy. In particular, *first-order* transitions are associated with inflection points in $\beta(E)$ that have a positive slope. Therefore, it can easily be identified by a positive-valued peak in the energy derivative $\gamma(E) = d\beta(E)/dE$. Similarly, a *second-order* transition occurs if $\gamma(E)$ attains a negative-valued peak. Examples of microcanonical *first-* and *second-order* transition signals are shown in Fig. 1. The extension of this method towards the identification of higher-order transitions is possible and will be described elsewhere [60].

It should be noted that different definitions of the microcanonical entropy $S(E)$ exist, but the differences have virtually no impact on the quantitative analysis of the cooperative behavior in transition regions because of the abrupt change of the density of states in the corresponding energetic ranges (for reviews see, e.g., Refs. [3, 43, 69, 70]).

III. RESULTS

Single flexible elastic homopolymers generally exhibit three distinct structural phases. In the high-temperature gas-like regime, typical conformations resemble extended, random coils. With decreasing temperature, the system first undergoes the Θ collapse transition into the liquid-like compact globular phase, and finally freezes into the solid "crystalline" phase. From our simulations of the

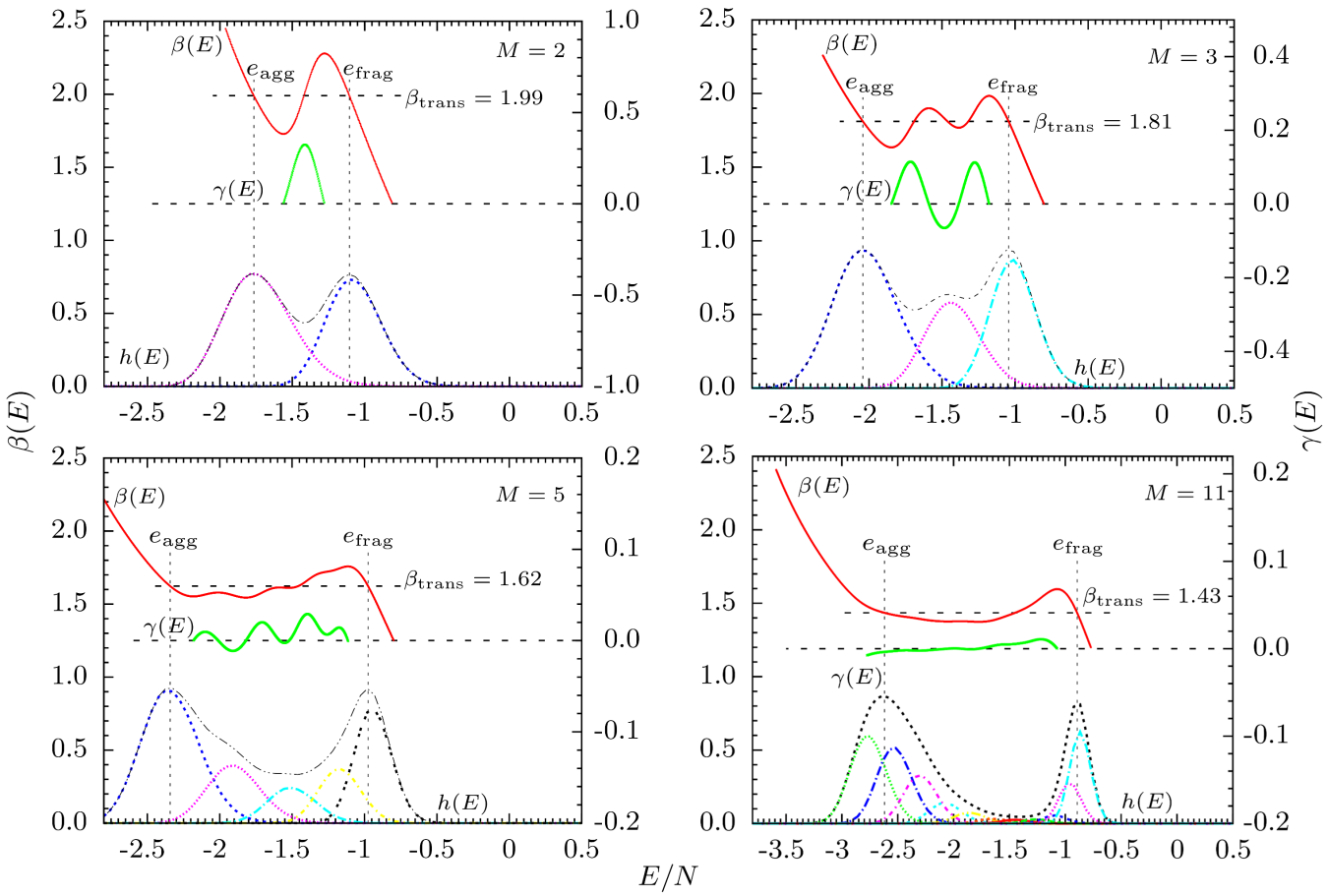

FIG. 2. Microcanonical temperature $\beta(E)$ and its energy derivative $\gamma(E)$ for systems with $M = 2, 3, 5, 11$ oligomers with $N = 5$ monomers each. The dashed vertical lines $e_{\rm agg}$ and $e_{\rm frag}$ outline the aggregation transition region. The upper horizontal dashed line provides an estimate for the inverse aggregation temperature $\beta_{\rm agg}$. The oscillations in $\beta(E)$ reveal the sequential nature of the transition and correspond to individual subtransitions. The unimodal canonical energy histograms of the subphases $h_i(E;\beta_{\rm agg})$ are also shown. The envelope of the subphase histograms represents the thermodynamically relevant canonical distribution of energetic states at the transition temperature, $h(E;\beta_{\rm agg})$. The absolute scale of these distributions is arbitrary.

multi-chain model employed in this study, we find that the prominent aggregation transition is accompanied by the collapse of the individual chains, and the two transitions are not separate processes. This has also been observed in the case of semi-flexible homopolymers [44]. However, in contrast to heteropolymer systems [45], the freezing transition occurs at temperatures well below the aggregation transition. In fact, at low temperatures, the thermodynamic properties of a multi-chain system are very similar to those of a single polymer chain with identical (total) number of monomers MN.

A. Microcanonical analysis of aggregation transitions

In this section, we discuss the properties of aggregation transitions from the perspective of microcanonical analysis. We systematically examine systems consisting of up to $M = 20$ individual chains with fixed length of $N = 5$ monomers. Brief inspection of the microcanonical quantities for four system sizes in Fig. 2 suggests that for finite systems the aggregation transition is a first-order process, as expected. The microcanonical inverse temperature curves $\beta(E)$ show a prominent back-bending region accompanied by positive-valued peaks in $\gamma(E)$. The low-energy aggregate phase is energetically separated from the disordered fragmented phase by an amount corresponding to the latent heat $\Delta q = e_{\rm frag} - e_{\rm agg}$, represented in Fig. 2 by the separation between the two dashed vertical lines. Finally, the combined canonical histograms $h(E;\beta_{\rm agg})$, also shown in Fig. 2, exhibit bimodality which is characteristic of first-order transitions in finite systems.

Closer inspection of the back-bending region of $\beta(E)$ reveals additional oscillations. It is evident that their number is proportional to the number of individual chains in the system. This observation motivates the description of the aggregation transition as a series of subtransitions between intermediate structural phases. Here we define the term "subphase" to represent a distinct

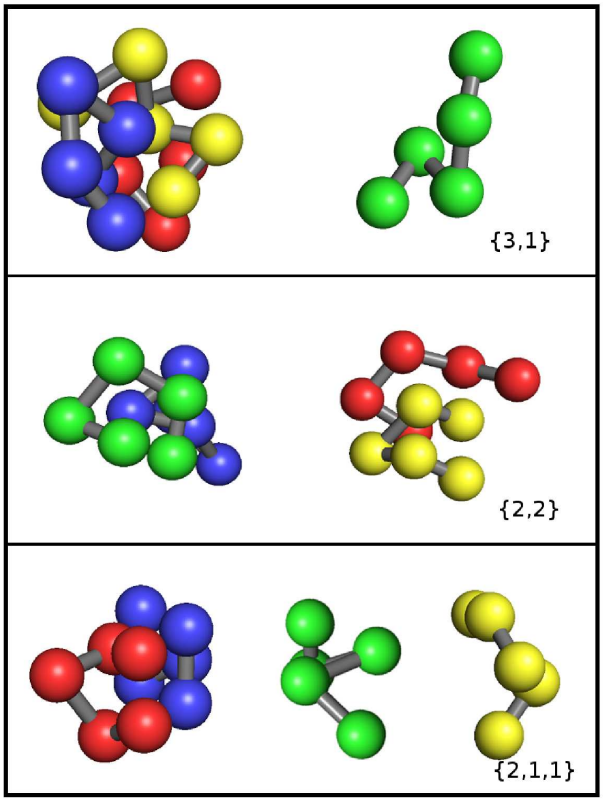

FIG. 3. Sample configurations of intermediate subphases found at the aggregation temperature in a system consisting of four chains with five monomers each. Due to entropic suppression, the $\{2,2\}$ subphase has an unexpectedly small canonical probability $p_{\{2,2\}}(\beta_{\rm agg}) < 0.007$, and is the first example of a *missing* (or entropically strongly suppressed) subphase in the aggregation process of the multi-chain system.

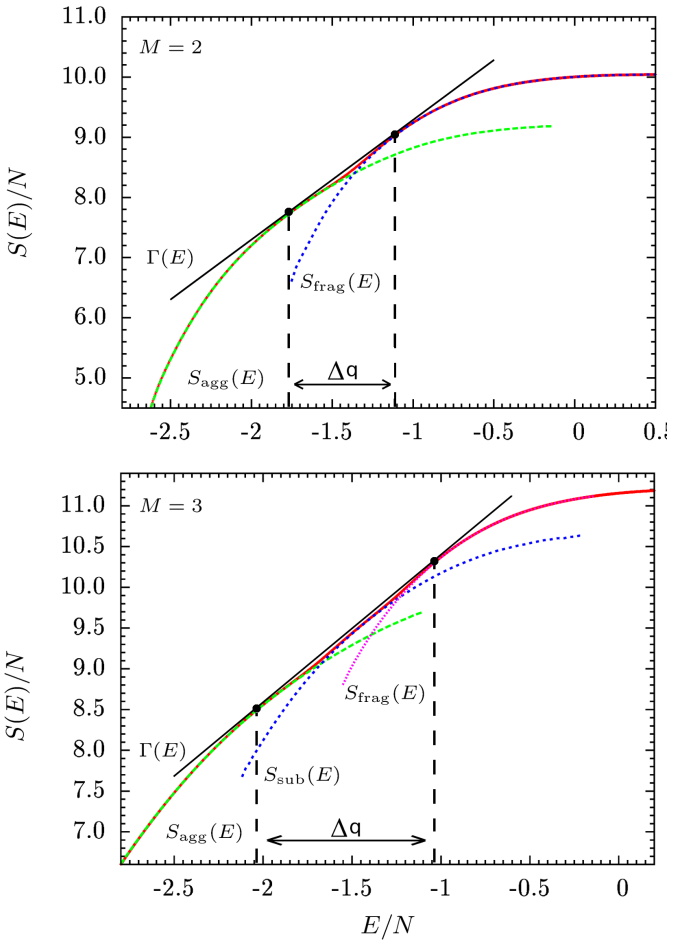

FIG. 4. Microcanonical entropy per monomer $S(E)$ (solid) and the individual subphase entropies (dotted) for systems with $M = 2, 3$ chains. The double-tangent $\Gamma(E)$ represents the Gibbs hull, the slope of which provides an estimate for the inverse transition temperature $\beta_{\rm agg}$.

grouping of partially formed aggregates. As shown in Fig. 3, a system of $M = 4$ chains can form three intermediate subphases $\{\{3,1\},\{2,2\},\{2,1,1\}\}$, where the number of elements in each set corresponds to the number of non-interacting partial clusters, and the numerical values represent the number of chains in each cluster. Previous studies suggest that subtransitions occur between these partially fragmented subphases [42–45]. However, this analysis was performed mostly on the level of visual inspection of individual system configurations. For a more quantitative approach, we have implemented a structure-detection algorithm capable of classifying configurations based on the number and size of partially formed aggregates. This allows us to collect separate statistical data for each subphase and to determine their relative frequency. The total density of states of a system in the transition region can be expressed as the sum of contributions from individual subphases

$$g(E) = \sum_i g_i(E). \tag{14}$$

The probability of finding a system in the i-th subphase at a fixed energy E can then be written as

$$p_i(E) = \frac{g_i(E)}{g(E)}. \tag{15}$$

The logarithm of the density of states, the microcanonical entropy $S(E)$, cannot be expressed as a sum of individual subphase entropies. Instead

$$S(E) = k_{\rm B} \ln \sum_i e^{S_i(E)/k_{\rm B}}, \tag{16}$$

where $S_i(E) = k_{\rm B} \ln g_i(E)$. In Fig. 4, the microcanonical entropy $S(E)$ (solid) and the individual subphase entropy curves (dashed) are shown for systems of $M = 2$ and $M = 3$ chains. For $M = 2$, aggregation is a single-step transition between the fragmented and the aggregate phase. When the aggregate is dissociated into two weakly interacting chains, the system gains an amount of entropy approximately equal to the translational entropy of a single chain $S_{\rm trans} \sim \ln V$, where V is the

volume of the simulation sphere. This increase in entropy is apparent from the vertical separation between $S_{\rm agg}$ and $S_{\rm frag}$. The changes in conformational entropy are negligible in comparison to the translational entropy and will not be discussed here. When $M = 3$, in addition to the aggregate and fragmented phases, a single subphase $\{2, 1\}$ can be formed. As a result, aggregation becomes a two-step process, each decreasing the entropy by an amount $\sim S_{\rm trans}$. We note that the entropy curves of the individual subphases are strictly concave. It is the vertical displacement between the curves, due to changes in translational entropy, that is ultimately responsible for the origin of the convex intruder in the microcanonical entropy $S(E)$ and consequently for the back-bending feature in $\beta(E)$, signaling the first-order character of the aggregation transition.

Differentiating Eq. (16) with respect to energy gives a simple expression for the microcanonical inverse temperature $\beta(E)$ in terms of the inverse temperatures of the individual subphases:

$$\beta(E) = \frac{\sum_i \beta_i e^{S_i(E)/k_{\rm B}}}{\sum_i e^{S_i(E)/k_{\rm B}}} = \sum_i p_i(E)\beta_i(E). \qquad (17)$$

Hence in the transition region, $\beta(E)$ can be interpreted as the weighted sum of the inverse subphase temperatures with respect to the multicanonical probabilities from Eq. (15). At a fixed energy E, the system can be found in one of the distinct subphases with a respective inverse temperature $\beta_i(E)$. In general, $\beta_i(E) \neq \beta(E)$. However setting the energy derivative of Eq. (15) to zero, we find that $\beta_i(E) = \beta(E)$ precisely when the probability of a given subphase $p_i(E)$ attains its maximum value. The oscillations in $\beta(E)$ arise from the changes in the relative weights $p_i(E)$ in the back-bending region.

In Fig. 4, we also show the double-tangent (Gibbs hull) $\Gamma(E)$. Its slope is the appropriate quantity for the estimation of the aggregation transition temperature $\beta_{\rm agg}$. In Table I, $\beta_{\rm agg}$ is listed for system sizes of up to $M = 20$ chains. In single-step first-order transitions, the slope of $\Gamma(E)$ coincides with the inverse temperature obtained by Maxwell construction. However, in composite multi-step transitions, the location of the Maxwell construction becomes ambiguous due to multiple oscillations of $\beta(E)$.

B. Entropically suppressed subphases

In the following, we discuss the results of the analysis of canonical energy histograms $h(E; \beta_{\rm agg})$, shown alongside the microcanonical quantities in Fig. 2. The histogram $h(E; \beta_{\rm agg})$, collected at the inverse aggregation temperature $\beta_{\rm agg}$, can be expressed as a sum of contributions from individual subphases

$$h(E; \beta_{\rm agg}) = \sum_i h_i(E; \beta_{\rm agg}), \qquad (18)$$

TABLE I. Inverse aggregation temperature ($\beta_{\rm agg}$), energy per monomer in the aggregate phase ($e_{\rm agg}$), energy per monomer in the fragmented phase ($e_{\rm frag}$), and the latent heat per monomer (Δq). The uncertainty for all listed quantities is ± 0.5 in the last decimal.

System ($M \times N$)	$\beta_{\rm agg}$	$e_{\rm agg}$	$e_{\rm frag}$	Δq
2×5	1.99	-1.77	-1.11	0.67
3×5	1.81	-2.04	-1.04	1.00
4×5	1.70	-2.22	-1.01	1.22
5×5	1.62	-2.35	-0.98	1.37
8×5	1.51	-2.56	-0.93	1.63
11×5	1.43	-2.62	-0.89	1.73
20×5	1.35	-2.80	-0.85	1.95

TABLE II. Theoretical number of subphases ($N_{\rm sub}$); not including the fully aggregated and fragmented phases, number of significantly represented subphases ($\hat{N}_{\rm sub}$), and the total contribution of the "missing" subphases towards the canonical distribution $h(E; \beta_{\rm agg})$ at the inverse transition temperature $\beta_{\rm agg}$.

System ($M \times N$)	$N_{\rm sub}$	$\hat{N}_{\rm sub}$	$\sum p_{\rm miss}$
3×5	1	1	N/A
4×5	3	2	< 0.007
5×5	5	3	< 0.014
11×5	54	9	< 0.026
20×5	625	18	< 0.028

where the canonical histograms of the subphases are related to their contributions towards the density of states via

$$h_i(E; \beta_{\rm agg}) \propto g_i(E) e^{-\beta_{\rm agg} E}. \qquad (19)$$

At all system sizes, the aggregate and fragmented phases have the largest canonical probability and are energetically well separated. The intermediate subphases have overlapping energy distributions and occur with smaller probabilities. The energetic separation of the aggregate and fragment phases in combination with the loss of translational and conformational entropy, as well as the suppression of certain classes of intermediate-size clusters for larger systems, lead to the formation of an entropic depletion zone characteristic for first-order-like transitions in finite systems.

A striking feature emerges for systems with $M > 3$ chains. Already for $M = 4$ (see Fig. 5), we notice that the subphase consisting of two clusters $\{2, 2\}$ appears with unexpectedly small canonical probability $p_{\{2,2\}}(\beta_{\rm agg}) < 0.007$. That only certain subphases contribute significantly towards the canonical energy histograms, becomes even more apparent for larger systems. In Table II, we list the theoretical values for the number of

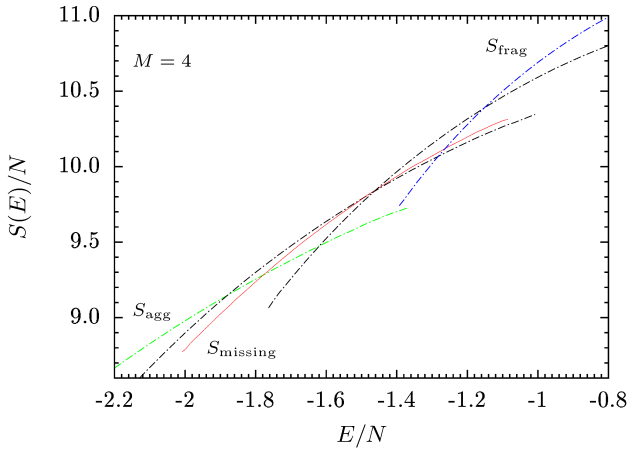

FIG. 5. Subphase entropy curves (patterned) in the aggregation transition region for a system of $M = 4$ oligomers. The entropically suppressed *missing* subphase $\{2, 2\}$ is highlighted in red (solid).

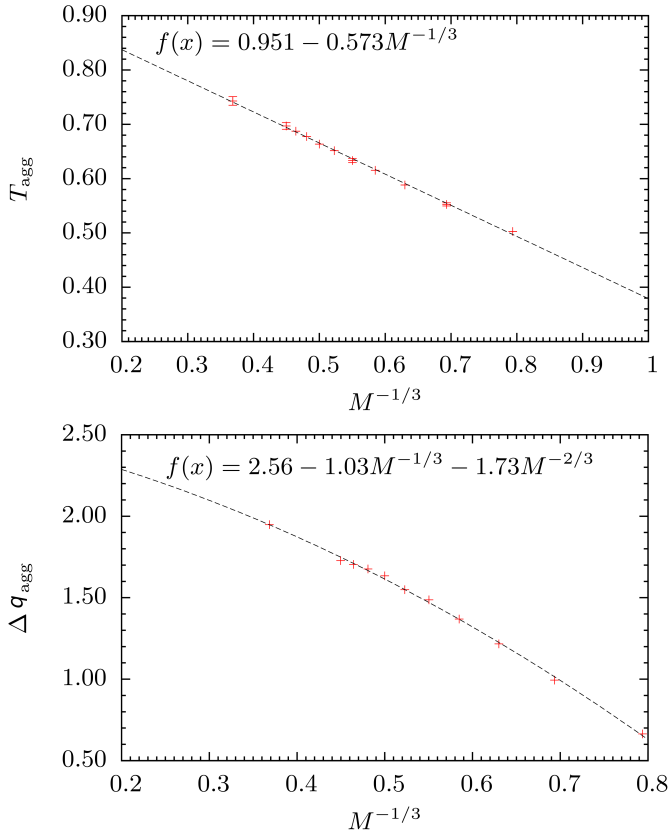

FIG. 6. Scaling behavior of the aggregation transition temperature $T_{\rm agg}$ and the latent heat per monomer $\Delta q_{\rm agg}$, with respect to $M^{-1/3}$ where M is the number of polymer chains. The latent heat increases with system size, providing further evidence that the transition remains of first order even for large M.

possible subphases ($N_{\rm sub}$) alongside the number of subphases that were detected with non-negligible probability ($\hat{N}_{\rm sub}$). The total contribution of the *missing* subphases towards the canonical energy histograms $h(E; \beta_{\rm agg})$ is less then $\approx 3\%$ despite the fact that the number of the subphases grows rapidly with system size. The observed results suggest that a system of M chains is most often found in a small subset of $(M-2)$ subphases, each consisting of K individual chains and a cluster of $(M-K)$ chains. In fact, for $M < 8$ we observe $(M-1)$ oscillations in the inverse microcanonical temperature $\beta(E)$, showing that the aggregation transition consists of a sequence of $(M-1)$ distinct subtransitions, each corresponding to a single chain breaking off the main aggregate. However in larger systems, some of the subtransitions overlap in energy and cannot be associated with individual oscillations of $\beta(E)$. In order to better understand the reason behind the *missing* subphases, we first consider the effects of energy and translational entropy on the relative positions of subphase entropy curves $S_i(E)$. A reduction in the number of intra-chain interactions leads to the increase in energy, and as a result, subphases with a higher degree of fragmentation have their entropy curves shifted to higher energies. The number of independent fragments in a subphase determines its translational entropy and largely the vertical position of its entropy curve.

Closer look at Eq. (16) reveals that only those subphases whose entropy curves are closest to the total entropy $S(E)$, contribute significantly. Therefore an increase in energy of a subphase must be compensated by a sufficient increase in its translational entropy. Not surprisingly, the $(M-2)$ most frequent subphases consist of K individual chains and a single cluster of $(M-K)$ chains, maximizing translational entropy while maintaining a relatively high number of inter-chain interactions. In Fig. 5, we provide an example of the first missing subphase in a system of $M = 4$ chains. It is clear that except for a very narrow energy interval, the $\{2, 2\}$ subphase is depleted by the lower-energy $\{3, 1\}$ and the higher-entropy $\{2, 1, 1\}$ subphases (see Fig. 3). As the system size increases, the number of *missing* subphases increases rapidly, while the number of subphases with substantial canonical probabilities remains linearly proportional to M.

C. Scaling properties

It is also interesting to discuss the dependence of the aggregation temperature $T_{\rm agg} = \beta_{\rm agg}^{-1}$, and the associated latent heat per monomer $\Delta q = e_{\rm frag} - e_{\rm agg}$, on the system size M. Previous studies have addressed in detail the effects of system size and the particle density ρ on the transition temperature [46, 47]. Here we keep the monomer density constant at $\rho = 10^{-3}$ and consider the scaling properties of $T_{\rm agg}$ and Δq only to obtain further evidence that the aggregation transition remains first-

order-like with increasing system size. In Table I, we have listed the values of $\beta_{\rm agg}$ and Δq for system sizes of up to $M = 20$ chains.

It has been argued (see, e.g., Refs. [71, 72]) that for transitions with entropic barrier, finite-size corrections scale like $f(\xi^{-1})$, where ξ is a characteristic thermodynamic length scale or structural order parameter. In our case, it is appropriate to choose the dimensionless variable $\xi = R_{\rm gyr}/r_0$, where $R_{\rm gyr}$ is the radius of gyration of the entire system and $r_0 = {\rm const}$ the intrinsic system length scale in our model. Near the transition point, most monomers assemble in a spherical shape and it is reasonable to assume that $R_{\rm gyr} \propto M^{1/3}$ [actually $(NM)^{1/3}$, but N is constant throughout this study]. Therefore, at constant density, we assume that the transition temperature for a finite number of chains M behaves like $T_{\rm agg}(M) = T_{\rm agg}^{M\to\infty} f(M^{-1/3})$, where $T_{\rm agg}^{M\to\infty}$ is the aggregation temperature in the limit of $M \to \infty$ chains at constant density. Assuming that the finite-size corrections to the aggregation transition temperature are mainly due to volume effects, we use the ansatz

$$T_{\rm agg}(M) \propto \alpha_0 + \alpha_1 M^{-1/3} + \mathcal{O}(M^{-2/3}). \qquad (20)$$

This behavior has been confirmed in a previous study on polymer aggregation in spherical confinement [46].

Due to the difference in the number of nearest-neighbor interactions between surface and bulk monomers, we expect the latent heat Δq to depend not only on the bulk volume occupied by the system, but also on its surface. Hence,

$$\Delta q(M) \propto \delta_0 + \delta_1 M^{-1/3} + \delta_2 M^{-2/3} + \mathcal{O}(M^{-1}). \qquad (21)$$

Data fits of the values from Table I are shown in Fig. 6. We observe that the transition temperature is reduced for small system sizes as finite-size effects become more prominent. For very large system sizes, it converges to a fixed value ($T_{\rm agg}^{M\to\infty} \approx 0.95$). The latent heat per monomer approaches the estimated value $\Delta q^{M\to\infty} \approx 2.56$ in the thermodynamic limit, providing further evidence that the aggregation transition is a first-order phase-separation process.

IV. SUMMARY

In this study, we have investigated the properties of the aggregation transition for systems consisting of up to $M = 20$ short flexible elastic homopolymer chains. Utilizing microcanonical inflection-point analysis, we have confirmed that the aggregation transition is a sequential process consisting of $M-1$ subtransitions between intermediate, partially fragmented structural phases. Each oscillation in the microcanonical inverse temperature curve indicates a single transition between two adjacent subphases. We have established the relationship between the microcanonical density of states $g(E)$ and the densities of states $g_i(E)$ corresponding to the individual subphases. From this, we have further derived similar expressions for the microcanonical entropy $S(E)$ and its energy derivative, the microcanonical inverse temperature $\beta(E)$. We have used those relationships to motivate the origins of the convex intruder in $S(E)$ and the prominent back-bending region in $\beta(E)$, both of which are indicators of a first-order process.

Canonical energy histograms $h_i(\beta; E)$, collected at the transition temperature $\beta_{\rm agg}$ for each individual subphase, confirm that certain subphases contribute only negligibly to the total canonical distribution. The origin of these *missing* subphases can be explained on the basis of the effects of translational entropy on the relative positions of the subphase entropy curves $S_i(E)$. The results of this study show that with increasing system size, the number of possible subphases increases rapidly, whereas their relevant subset increases only linearly.

Finally, we have discussed the scaling properties of $\beta_{\rm agg}$ and the latent heat per monomer Δq. The increasing values of Δq with system size provide further evidence that the aggregation transition seems to remain a first-order process even as M tends towards the thermodynamic limit.

ACKNOWLEDGMENTS

This work has been supported partially by the NSF under Grant Nos. DMR-1463241 and DMR-1207437, and by CNPq (National Council for Scientific and Technological Development, Brazil) under Grant No. 402091/2012-4.

[1] D. J. Selkoe, Nature **425**, 900 (2003).
[2] F. Chiti, and C. M. Dobson, Ann. Rev. of Biochemistry **75**, 333 (2006).
[3] M. Bachmann, *Thermodynamics and Statistical Mechanics of Macromolecular Systems*, (Cambridge University Press, Cambridge, 2014).
[4] E. Marinari and G. Parisi, Europhys. Lett. **19**, 451 (1992).
[5] A. P. Lyubartsev, A. A. Martsinovski, S. V. Shevkunov, and P. N. Vorontsov-Velyaminov, J. Chem. Phys. **96**, 1776 (1992).
[6] R. H. Swendsen and J.-S. Wang, Phys. Rev. Lett. **57**,

2607 (1986).
[7] C. J. Geyer, *Computing Science and Statistics: Proceedings of the 23rd Symposium on the Interface*, edited by E. M. Keramidas (Interface Foundation, Fairfax Station VA, 1991), 156.
[8] K. Hukushima and K. Nemoto, J. Phys. Soc. Jpn. **65**, 1604 (1996).
[9] K. Hukushima, H. Takayama, and K. Nemoto, Int. J. Mod. Phys. C**7**, 337 (1996).
[10] T. Neuhaus and J. S. Hager, Phys. Rev. E **74**, 036702 (2006).
[11] B. A. Berg and T. Neuhaus, Phys. Lett. B **267**, 249 (1991).
[12] B. A. Berg and T. Neuhaus, Phys. Rev. Lett. **68**, 9 (1992).
[13] W. Janke, Physica A **254**, 164 (1998).
[14] B. A. Berg, Comp. Phys. Commun. **153**, 397 (2003).
[15] B. A. Berg, *Markov Chain Monte Carlo Simulations* (World Scientific, Singapore, 2004).
[16] M. Bachmann, Phys. Scr. **87**, 058504 (2013).
[17] F. Wang and D. P. Landau, Phys. Rev. Lett. **86**, 2050 (2001).
[18] F. Wang and D. P. Landau, Phys. Rev. E **64**, 056101 (2001).
[19] T. Vogel, Y. W. Li, T. Wüst, and D. P. Landau, Phys. Rev. Lett. **110**, 210603 (2013).
[20] S. Schnabel, M. Bachmann, and W. Janke, J. Chem. Phys. **131**, 124904 (2009).
[21] I. Carmesin and K. Kremer, Macromolecules **21**, 2819 (1988).
[22] H. P. Deutsch and K. Binder, J. Chem. Phys. **94**, 2294 (1991).
[23] P. Grassberger, Phys. Rev. E **56**, 3682 (1997).
[24] T. Vogel, M. Bachmann, and W. Janke, Phys. Rev. E **76**, 061803 (2007).
[25] W. Paul, T. Strauch, F. Rampf, and K. Binder, Phys. Rev. E **75**, 060801(R) (2007).
[26] S. Schnabel, T. Vogel, M. Bachmann, and W. Janke, Chem. Phys. Lett. **476**, 201 (2009).
[27] M. P. Taylor, W. Paul, and K. Binder, J. Chem. Phys. **131**, 114907 (2009).
[28] M. P. Taylor, W. Paul, and K. Binder, Phys. Rev. E **79**, 050801(R) (2009).
[29] D. T. Seaton, T. Wüst, and D. P. Landau, Phys. Rev. E **81**, 011802 (2010).
[30] D. T. Seaton, S. Schnabel, D. P. Landau, and M. Bachmann, Phys. Rev. Lett. **110**, 028103 (2013).
[31] T. Koci, and M. Bachmann, Phys. Rev. E **92**, 042142 (2015).
[32] M. Bachmann and W. Janke, Phys. Rev. Lett. **95**, 058102 (2005).
[33] J. Krawczyk, T. Prellberg, A. L. Owczarek, and A. Rechnitzer, Europhys. Lett. **70**, 726 (2005).
[34] J. Luettmer-Strathmann, F. Rampf, W. Paul, and K. Binder, J. Chem. Phys. **128**, 064903 (2008).
[35] M. Möddel, M. Bachmann, and W. Janke, J. Phys. Chem. B **113**, 3314 (2009).
[36] L. Wang, T. Chen, X. Lin, Y. Liu, and H. Liang, J. Chem. Phys. **131**, 244902 (2009).
[37] A. D. Swetnam and M. P. Allen, Phys. Chem. Chem. Phys. **11**, 2046 (2009).
[38] T. Vogel and M. Bachmann, Phys. Rev. Lett. **104**, 198302 (2010).
[39] Y. W. Li, T. Wüst, and D. P. Landau, Phys. Rev. E **87**, 012706 (2013).
[40] M. Möddel, W. Janke, and M. Bachmann, Phys. Rev. Lett. **112**, 148303 (2014).
[41] T. Vogel, J. Gross, and M. Bachmann, J. Chem. Phys. **142**, 104901 (2015).
[42] C. Junghans, M. Bachmann, and W. Janke, Phys. Rev. Lett. **97**, 218103 (2006).
[43] C. Junghans, M. Bachmann, and W. Janke, J. Chem. Phys. **128**, 085103 (2008).
[44] C. Junghans, M. Bachmann, and W. Janke, Europhys. Lett. **87**, 40002 (2009).
[45] C. Junghans, W. Janke, and M. Bachmann, Comp. Phys. Commun. **182**, 1937 (2011).
[46] J. Zierenberg, M. Mueller, P. Schierz, M. Marenz, and W. Janke, J. Chem. Phys. **141**, 114908 (2014).
[47] J. Zierenberg, and W. Janke, Europhys. Lett. **109**, 28002 (2015).
[48] K. F. Lau and K. A. Dill, Macromolecules **22**, 3986 (1989).
[49] F. H. Stillinger, T. Head-Gordon, and C. L. Hirshfeld, Phys. Rev. E **48**, 1469 (1993);
[50] F. H. Stillinger and T. Head-Gordon, Phys. Rev. E **52**, 2872 (1995).
[51] A. Irbäck, C. Peterson, F. Potthast, and O. Sommelius, J. Chem. Phys. **107**, 273 (1997).
[52] H.-P. Hsu, V. Mehra, W. Nadler, and P. Grassberger, J. Chem. Phys. **118**, 444 (2003).
[53] M. Bachmann and W. Janke, Phys. Rev. Lett. **91**, 208105 (2003).
[54] S. Schnabel, M. Bachmann, and W. Janke, Phys. Rev. Lett. **98**, 048103 (2007).
[55] M. E. Fisher, Rep. Prog. Phys. **30**, 615 (1967).
[56] M. P. Taylor, P. P. Aung, and W. Paul, Phys. Rev. E **88**, 012604 (2013).
[57] J. C. S. Rocha, S. Schnabel, D. P. Landau, and M. Bachmann, Phys. Rev. E **90**, 022601 (2014).
[58] M. P. Taylor and J. Luettmer-Strathmann, J. Chem. Phys. **141**, 204906 (2014).
[59] S. Schnabel, D. T. Seaton, D. P. Landau, and M. Bachmann, Phys. Rev. E **84**, 011127 (2011).
[60] K. Qi, and M. Bachmann, to be published (2016).
[61] F. Schmid, *Theory and Simulation of Multiphase Polymer Systems: Handbook of Multiphase Polymer Systems*, edited by A. Boudenne, L. Ibos, Y. Candau, and S. Thomas (John Wiley & Sons Ltd, Chichester UK, 2011), 31.
[62] R. B. Bird, C. F. Curtiss, R. C. Armstrong, and O. Hassager, *Dynamics of Polymeric Liquids*, 2nd ed. (Wiley, New York, 1987).
[63] K. Kremer and G. S. Grest, J. Chem. Phys. **92**, 5057 (1990).
[64] A. Milchev, A. Bhattacharya, and K. Binder, Macromolecules **34**, 1881 (2001).
[65] J. Gross, T. Neuhaus, T. Vogel, and M. Bachmann, J. Chem. Phys. **138**, 074905 (2013).
[66] A. M. Ferrenberg and R. H. Swendsen, Phys. Rev. Lett. **63**, 1195 (1989).
[67] S. Kumar, D. Bouzida, R. H. Swendsen, P. A. Kollman, and J. M. Rosenberg, J. Comput. Chem. **13**, 1011 (1992).
[68] P. M. Stevenson, Phys. Rev. D **23**, 2916 (1981).
[69] D. H. E. Gross, *Microcanonical Thermodynamics* (World Scientific, Singapore, 2001).
[70] P. Hänggi, S. Hilbert, and J. Dunkel, Phil. Trans. R. Soc. A **374**, 20150039 (2015).

[71] V. Privman and J. Rudnick, J. Stat. Phys. **60**, 551 (1990).
[72] C. Borgs and R. Kotecky, J. Stat. Phys. **79**, 43 (1995).